INT. J. NUM. METH. HEAT FLUID FLOW, VOL. 5, 481–494 (1995)

LINEAR STABILITY ANALYSIS OF THERMOCAPILLARY CONVECTION IN LIQUID BRIDGES USING A MIXED FINITE DIFFERENCE-SPECTRAL METHOD

J.-C. CHEN AND S.-S. SHEU

Department of Mechanical Engineering, National Central University, Chung-Li, Taiwan 32054, ROC

ABSTRACT

A linear stability analysis has been employed to investigate the thermocapillary instability occurring in a nonisothermal liquid bridge. The steady, axisymmetric basic state was solved numerically using a finite difference method. A mixed finite difference-spectral method, combining the advantages of both methods, was then used to reduce the linear disturbance equations to an eigenvalue problem. The critical Marangoni numbers for axisymmetric disturbances are predicted for small Prandtl numbers and various aspect ratios. The effect of surface heat transfer is also investigated. The present results are compared with energy-theory results and with the results of other experiments.

KEY WORDS Thermocapillary instability Spectral method Finite difference Eigenvalues

In order to avoid container contamination, the float-zone method has been widely used in the growth of high-purity crystals. Using this technique, many materials with high surface tensions have been successfully melted and recrystallized into single crystals. The size of the melt is restricted by capillary instability that originates at the meniscus, and the convection transports present in the melt during the growth strongly influence the structure and quality of individual crystals.

Two types of natural convection may occur in the melt due to the nonuniform temperature distribution: buoyancy-driven flow induced by the density gradient inside the melt, and thermocapillary flows caused by the surface-tension gradient at the gas–liquid interface. The influence of thermocapillary convection is dominant for microgravity environments or small-scale systems. The existence of thermocapillary convection in the melt of the float-zone process has been verified experimentally by Schwabe *et al.*[1]. Periodic striations in single molybdenum (Mo) crystals induced by the oscillatory thermocapillary flow have been reported by Jurisch and Löser[2].

In order to understand the transport phenomena, the float zone is simulated by vertical liquid bridges held between two concentric, cylindrical solid rods. The steady, axisymmetric thermocapillary flow in liquid bridges has been studied theoretically by several authors. Xu and Davis[3] and Kuhlmann[4] had treated this problem analytically. Numerical studies have been undertaken by Chang and Wilcox[5], Fu and Ostrach[6], and Chen *et al.*[7]. Experiments on thermocapillary convection in liquid bridges performed by Chun[8], Preisser *et al.*[9], Kamotani *et al.*[10] and Velten *et al.*[11] have shown that a steady axisymmetric flow may change into an oscillatory flow when the Marangoni number exceeds a critical value. Both axisymmetric and non-axisymmetric modes were observed, depending on the aspect ratio of the liquid bridge and the properties of the fluid. However, numerical solutions for a steady axisymmetric

0961–5539/95/060481–14$2.00

Received October 1993
Revised April 1994

thermocapillary flow can be obtained far beyond the critical Marangoni numbers obtained in experiments. Xu and Davis[12] used linear stability theory to study the stability of thermocapillary convection in a slender bridge (a zero aspect ratio). Their study did not include the effect created by the existence of the endwall boundary layer, and their results showed that the oscillatory flow may be induced by the thermocapillary force. But the critical Marangoni number they calculated is far below those obtained in experiments. Rupp, Müller and Neumann[13] have determined the critical Marangoni values using time-dependent, three-dimensional numerical modelling.

Since the basic-state velocity and temperature fields are two dimensional, the stability of thermocapillary convection in liquid bridges of finite aspect ratio is governed by partial-differential equations. Therefore, the stability analyses require a complex procedure to reduce the partial-differential equations to an eigenvalue system. Neitzel and his co-workers[14–16] employed both an energy stability analysis and a linear stability analysis to investigate this problem of O(1) aspect ratio. Their results showed that the critical Marangoni numbers predicted by the non-axisymmetric modes are much smaller than those obtained by the axisymmetric mode. In their approach, huge matrix systems are formed since the finite difference method with a staggered-grid discretization scheme is used to reduce the partial-differential disturbance equations to an eigenvalue system. Therefore, their solution procedure requires large computer memory and computation time.

The advantage of using a spectral scheme is that relatively few degrees of freedom are needed to approximate a given function, which reduces both computer storage requirements and computation time. In addition, the finite difference methods are easier to formulate for most kinds of boundary conditions. A mixed finite difference-spectral method combining the advantages of both methods has been used successfully to study the buoyancy convection in the finite box[17].

In the present study, linear stability analysis is carried out to study the instability of thermocapillary convection in liquid bridges of finite aspect ratio. The gas–liquid interface is assumed to have no surface deformation due to the presence of a large mean surface tension. The steady, axisymmetric basic state is determined numerically using a finite difference method applied to a streamfunction-vorticity-temperature formation. The disturbances are assumed to be infinitesimal and axisymmetric. A mixed finite difference-spectral method is employed to reduce the linear disturbance equations to an eigenvalue problem. The finite difference method is employed in the radial direction, and the spectral-Galerkin method is employed in the axial direction. The critical Marangoni numbers are determined for different aspect ratios, and the influence of the fluid properties and heating conditions on the stability properties are taken into consideration. The present results are compared with critical Marangoni numbers from recent laboratory experiments and also with the previous energy-stability results.

BASIC STATE

The problem examined in this study is essentially that treated by Chen *et al.*[7]. Consider an axisymmetric liquid bridge held between two coaxial rods of radius R separated by a distance L. The bridge contains an incompressible, Newtonian liquid. The thermocapillary flow in the bridge is driven by a temperature difference ΔT imposed across the rigid walls (at $z = 0$ and $z = L$), with the upper rod being at a higher temperature than the lower. The z direction has been selected as opposite the direction of gravity. The gas–liquid interface is bounded by an inviscid gas of negligible density and viscosity with temperature distribution $f(z)$, and it is assumed to have a large mean surface tension resulting in no surface deformation. The Boussinesq approximation is assumed to be valid and the surface tension is considered as a linear decreasing function of temperature.

The length, time, velocity, and pressure have been scaled by R_0, $R_0\mu/(\gamma_s\Delta T)$, $\gamma_s\Delta T/\mu$, and

$\Delta T/R_0$, respectively, where γ_s is the rate of decrease of surface tension with temperature and μ is the dynamic viscosity. The dimensionless temperature is defined by (temperature $- T_m)/\Delta T$, where T_m is the average temperature of the two rigid walls. We seek a steady, axisymmetric thermocapillary flow solution of the form $(u, v, w, p, T) = (U(r, z), 0, W(r, z), P(r, z), \Theta(r, z))$ where (u, v, w) are velocities corresponding to the usual cylindrical coordinates (r, θ, z), p is the pressure, and T is the temperature. By eliminating the pressure, the dimensionless governing equations can be expressed in the following form:

$$Re(r^{-1}\Psi_z\Omega_r - r^{-1}\Psi_r\Omega_z - r^{-2}\Psi_z\Omega) = \Omega_{rr} + r^{-1}\Omega_r - r^{-2}\Omega - Gr\,Re^{-1}\Theta \tag{1a}$$

$$Ma(r^{-1}\Psi_z\Theta_r - r^{-1}\Psi_r\Theta_z) = \Theta_{rr} + r^{-1}\Theta_r + \Theta_{zz} \tag{1b}$$

$$r\Omega = \Psi_{rr} - r^{-1}\Psi_r + \Psi_{zz} \tag{1c}$$

where the stream function ψ and vorticity ω are defined as:

$$U = r^{-1}\Psi_z, \qquad W = -r^{-1}\Psi_r, \qquad \Omega = U_z - W_r \tag{2}$$

The boundary conditions are:

$$\Psi = 0, \Omega = r^{-1}\Psi_{zz}, \Theta = -0.5 \qquad \text{at } z = 0 \tag{3}$$

$$\Psi = 0, \Omega = r^{-1}\Psi_{zz}, \Theta = 0.5 \qquad \text{at } z = 1/A \tag{4}$$

$$\Psi = 0, \Omega = 0, \Theta_r = 0 \qquad \text{at } r = 0 \tag{5}$$

$$\Psi = 0, \Omega = \Theta_z, \Theta_r = -Bi[\Theta - f(z)] \qquad \text{at } r = 1 \tag{6}$$

The dimensionless parameters appearing in governing equations and boundary conditions are:

$$Re = \gamma_s\Delta T R_0/(\mu\nu) \quad \text{(Reynolds number)}$$

$$Ma = Re\,Pr = \gamma_s\Delta T R_0/(\mu\alpha) \quad \text{(Marangoni number)},$$

$$Gr = g\beta\Delta T R_0^3/\nu^2 \quad \text{(Grashof number)}$$

$$Bi = h_g L/k \quad \text{(Biot number)}$$

$$A = R/L \quad \text{(aspect ratio)}$$

where ν is the kinematic viscosity, α is the thermal diffusivity, β is the thermal expansion coefficient, h_g is the surface heat transfer coefficient, k is the thermal conductivity, and Pr is the Prandtl number. The ambient temperature distributions are assumed to be:

(I) $$f(z) = -0.5$$

and

(II) $$f(z) = Az - 0.5$$

respectively. Case (I), employed by Neitzel and his co-workers[14–16], represents that the surroundings are at constant temperature equal to that of the cold rod, case (II), used by Xu and Davis[3], shows that the surrounding temperature varies linearly from the cold wall to the hot wall.

We solved (1) with conditions (3)–(6) by applying a central-difference method with second-order accuracy. The solution procedure is a modified version of that employed by and Chen *et al.*[18] and Chen *et al.*[7]. The details of the numerical method appear in the solutions and will not be repeated here.

LINEAR STABILITY ANALYSIS

The equations governing infinitesimal, axisymmetric disturbances of the flow are obtained by

substituting:

$$(u, v, w, p, T) = [U(r, z), 0, W(r, z), P(r, z), \Theta(r, z)] + [u'(t, r, z), 0, w'(t, r, z), p'(t, r, z), T'(t, r, z)] \quad (7)$$

into the unsteady governing equations, eliminating the portion resulting solely from the basic state and neglecting second- and higher-order terms. We make the usual assumption that the disturbance may be decomposed into normal modes as:

$$(u', w', p', T') = (\tilde{u}, \tilde{w}, \tilde{p}, \tilde{T}) \exp(\sigma t) \quad (8)$$

The complex eigenvalue:

$$\sigma = \gamma + i\omega$$

contains the growth rate γ and the angular frequency ω. The real part of σ determines the stability ($\gamma < 0$) or instability ($\gamma > 0$) of the basic state. The condition $\gamma = 0$ corresponds to marginal stability.

Substituting (8) into the linearized governing equations and dropping the overtildes of $\tilde{u}$, $\tilde{w}$, $\tilde{p}$ and $\tilde{T}$, we obtained the following set of partial differential equations:

$$u_r + r^{-1}u + w_z = 0 \quad (9a)$$

$$Re[\sigma u + Uu_r + Wu_z + U_r u + U_z w] = -p_r + u_{rr} + r^{-1}u_r + u_{zz} - r^{-2}u \quad (9b)$$

$$Re[\sigma w + Uw_r + Ww_z + W_r u + W_z w] = p_z + w_{rr} + r^{-1}w_r + w_{zz} + Gr\,Re^{-1}T \quad (9c)$$

$$Ma[\sigma T + UT_r + WT_z + \Theta_r u + \Theta_z w] = T_{rr} + r^{-1}T_r + T_{zz} \quad (9d)$$

Eliminating the disturbance pressure yields:

$$\begin{aligned}\sigma Re(r^{-1}\psi_{zz} + r^{-1}\psi_{rr} - r^{-2}\psi_r) - r^{-1}\psi_{rrrr} + (2r^{-2} + Re\,Ur^{-1})\psi_{rrr} \\ + \left[Re\,r^{-1}(U_r + W_z) - 2Re\,r^{-2}U - 3r^{-2} + Re\,Wr^{-1}\frac{\partial}{\partial z} - 2r^{-1}\frac{\partial^2}{\partial z^2}\right]\psi_{rr} \\ + \left[3r^{-4} + 2Re\,Ur^{-3} - Re\,r^{-2}(U_r + W_z) - Re\,r^{-1}(U_{zz} - W_{rz})\right. \\ \left. - Re\,Wr^{-2}\frac{\partial}{\partial z} + (2r^{-2} + Re\,Ur^{-1})\frac{\partial}{\partial z^2}\right]\psi_r \\ + [Re\,r^{-1}(U_{rz} - W_{rr}) - Re\,r^{-2}(U_z - W_r)]\psi_z \\ + [Re\,r^{-1}(U_r + W_z) - Re\,Ur^{-2}]\psi_{zz} \\ + Re\,Wr^{-1}\psi_{zzz} - r^{-1}\psi_{zzzz} + Gr\,Re^{-1}T_r = 0 \end{aligned} \quad (10a)$$

$$\sigma Ma\,T + Ma[UT_r + WT_z + r^{-1}\Theta_r\psi_z - r^{-1}\Theta_z\psi_r] = T_{rr} + r^{-1}T_r + T_{zz} \quad (10b)$$

with the boundary conditions

$$\psi = \psi_z = T = 0 \quad \text{at } z = 0, z = 1/A \quad (11)$$

$$\psi = \psi_r = T_r = 0 \quad \text{at } r = 0 \quad (12)$$

$$\psi = 0, \psi_{rr} - r^{-1}\psi_r = -T_z, T_r = -Bi\,T \quad \text{at } r = 1 \quad (13)$$

The disturbance stream function ψ is defined as

$$u = r^{-1}\psi_z, \qquad w = -r^{-1}\psi_r$$

Equations (10) and boundary conditions (11)–(13) form a linear partial differential eigenvalue problem which will have a non-trivial solution, but for only certain parameter values.

NUMERICAL PROCEDURE

The mixed finite difference-spectral method, which has been used successfully to compute the linear Marangoni instability of fluids in circular cylindrical containers[19], has been modified to solve the linear partial differential eigenvalue system (10)–(13). In the present problem, the complexity of the boundary conditions at $r=1$ prohibits the use of a Galerkin expansion in the r direction. To avoid this difficulty, finite-differencing is used in the r direction and a spectral-Galerkin procedure is employed in the z direction.

The disturbance stream function and the disturbance temperature are expressed in the form:

$$\psi = \sum_{j}^{N} A_j(z)\psi_j(r) \tag{14a}$$

$$T = \sum_{j}^{N} B_j(z)T_j(r) \tag{14b}$$

where N is the total number of the trial-function terms. The trial functions A_j and B_j were chosen as the following forms:

$$A_j(z) = \frac{\cosh \lambda_j(Az - \frac{1}{2})}{\cosh \frac{\lambda_j}{2}} - \frac{\cos \lambda_j(Az - \frac{1}{2})}{\cos \frac{\lambda_j}{2}} \tag{15a}$$

$$B_j(z) = \cos(Az - \tfrac{1}{2})j\pi \tag{15b}$$

where λ_j is the root of

$$\tanh \lambda/2 + \tan \lambda/2 = 0 \tag{16}$$

A_j are the beam functions developed by Harris and Reid[20]. The series (14) is substituted into the linear disturbance equations (10), which are then multiplied by $A_k(z)$ and $B_k(z)$ $(k = 1, \ldots, N)$, respectively, and integrated over the region of $0 < z < 1/A$ to obtain a set of $2N$ linear ordinary differential equations for the functions $\psi_j(r)$ and $T_j(r)$. We define:

$$\mathbf{S}(r) = [\psi_1(r), \psi_2(r), \psi_3(r), \ldots, \psi_j(r), \ldots, \psi_N(r)]^{\mathrm{T}} \tag{17a}$$

$$\mathbf{T}(r) = [T_1(r), T_2(r), T_3(r), \ldots, T_j(r), T_N(r)]^{\mathrm{T}} \tag{17b}$$

Then we obtain:

$$\sigma(\mathbf{N}_{11}D_r^2\mathbf{S} + \mathbf{N}_{12}D_r\mathbf{S} + \mathbf{N}_{13}\mathbf{S}) + \mathbf{M}_{11}D_r^4\mathbf{S} + \mathbf{M}_{12}D_r^3\mathbf{S} + \mathbf{M}_{13}D_r^2\mathbf{S} + \mathbf{M}_{14}D_r\mathbf{S} + \mathbf{M}_{15}\mathbf{S} + M_{16}D_r\mathbf{T} = \mathbf{0} \tag{18a}$$

$$\sigma\mathbf{M}_{21}\mathbf{T} + \mathbf{M}_{22}D_r\mathbf{S} + \mathbf{M}_{23}\mathbf{S} + \mathbf{M}_{24}D_r^2\mathbf{T} + \mathbf{M}_{25}D_r\mathbf{T} + \mathbf{M}_{26}\mathbf{T} = \mathbf{0} \tag{18b}$$

where $D_r = \mathrm{d}/\mathrm{d}r$, $D^2 = \mathrm{d}^2/\mathrm{d}r^2, \ldots$ etc. The corresponding boundary conditions become:

$$\mathbf{S} = D_r\mathbf{S} = D_r\mathbf{T} = \mathbf{0} \qquad \text{at } r = 0 \tag{19a–c}$$

$$\mathbf{S} = \mathbf{0}, D_r^2\mathbf{S} - D_r\mathbf{S} + \mathbf{M}_b\mathbf{T} = \mathbf{0}, D_r\mathbf{T} + Bi\mathbf{T} = \mathbf{0} \quad \text{at } r = 1 \tag{19d–f}$$

The $\mathbf{M}_{ij}$ and $\mathbf{N}_{ij}$ in Equation (18)–(19) are $N \times N$ matrices and list in the appendix.

The second-order central differencing is used to solve the linear ordinary differential system (18) together with boundary conditions (19). Let the region $0 < r < 1$ be divided into $M - 1$ equal intervals, with $i = 1$ and $i = M$ at the boundary points. The difference equations are:

$$\bar{\mathbf{M}}_{11}\mathbf{S}^{i+2} + \bar{\mathbf{M}}_{12}\mathbf{S}^{i+1} + \bar{\mathbf{M}}_{13}\mathbf{S}^{i} + \bar{\mathbf{M}}_{14}\mathbf{S}^{i-1} + \bar{\mathbf{M}}_{15}\mathbf{S}^{i-2} + \bar{\mathbf{M}}_{16}\mathbf{T}^{i+1} + \bar{\mathbf{M}}_{17}\mathbf{T}^{i-1} = \sigma(\bar{\mathbf{N}}_{11}\mathbf{S}^{i+1} + \bar{\mathbf{N}}_{12}\mathbf{S}^{i} + \bar{\mathbf{N}}_{13}\mathbf{S}^{i-1}) \tag{20a}$$

$$\bar{\mathbf{M}}_{22}\mathbf{S}^{i+1} + \bar{\mathbf{M}}_{23}\mathbf{S}^{i} + \bar{\mathbf{M}}_{24}\Sigma^{i-1} + \bar{\mathbf{M}}_{25}\mathbf{T}^{i+1} + \bar{\mathbf{M}}_{26}\mathbf{T}^{i} + \bar{\mathbf{M}}_{27}\mathbf{T}^{i-1} = \sigma\bar{\mathbf{M}}_{21}\mathbf{T}^{i} \tag{20b}$$

with the boundary conditions:

$$\mathbf{S}^{1} = 0, \mathbf{S}^{-1} = \mathbf{S}^{1}, \mathbf{T}^{-1} = \mathbf{T}^{1} \tag{21a–c}$$

$$\mathbf{S}^{M} = 0, \left(\frac{1}{\Delta r^2} - \frac{1}{\Delta r}\right)\mathbf{S}^{M+1} + \left(\frac{1}{\Delta r^2} + \frac{1}{\Delta r}\right)\mathbf{S}^{M-1} + M_b\mathbf{T}^{M} = 0,$$

$$\mathbf{T}^{M} = \frac{1}{2\Delta r Bi}(\mathbf{T}^{m-1} - \mathbf{T}^{M+1}) \tag{21d–f}$$

where $\Delta r = 1/(M-1)$. The definitions of the matrices $\bar{\mathbf{M}}_{ij}$ are described in Appendix B.

This yields to a generalized real eigensystem of the form:

$$\mathbf{KX} = \sigma\mathbf{MX} \tag{22}$$

In these equations, **X** is the transpose of the vector consisting of all unknowns on all grid points, **M** is a symmetric positive definite matrix, and **K** has a banded structure and depends on the basic state. The elements of **K** involving the single integrals are evaluated by Simpson's rule. The matrix eigenvalue problem (22) was solved using the IMSL subroutine DG2LRG which is developed according to a QZ algorithm.

If all eigenvalues have negative real parts, the basic state is stable. If the greatest real part of all eigenvalues is positive, the basic state is unstable. *Figure 1* shows the variation of the eigenvalue which has the greatest real part of all eigenvalues with Ma for fixed Pr, Bi, Gr, and A. The critical Marangoni number Ma_c is determined as the greatest real part of all eigenvalues is zero.

The value of the critical Marangoni number is strongly affected by the accuracy of the solution of the basic state. Therefore, a fine grid distribution is needed in the z direction since the boundary-layer thickness near the sidewalls decreases as Ma increases. Checks were carried out to determine the influence of the number of terms in Galerkin representation on the accuracy of the results. Checks were also carried out on various points in the finite-difference grid to determine how they influenced the accuracy of the results. The results for $Pr = 1$, $Bi = 0.3$, $Gr = 0$, $Ma = 2000$, and $A = 1$ are shown in *Figures 2* and *3*. In *Figure 2*, M and Nz represent the number of grid points in the r and z directions, respectively. In *Figure 2*, we see that the growth rate γ approaches a certain value when the number of grid points increases in both r and z directions. Basically, the finer grids will have more accurate results, but it requires more computation time. Obviously, the growth rate γ for the fixed numbers of the finite-difference grid points M asymptotically approaches a constant value as the number of trial-function terms N increases. In *Figure 3*, with the same number of trial function terms, the required CPU time for $M = 61$ is three times as large as it is for $M = 51$. The requirement of the computer memory increases significantly as M and N increase. For the results discussed below, the terms in the Galerkin expansion are fixed at 8 and the points in the finite-difference grids vary with the aspect ratio, which is the same as the grid points selected for the basic state in the z direction. The grid distributions for different aspect ratios used in the present study are listed in *Table 1*.

RESULTS AND DISCUSSION

The computations described in the previous section have been done in double-precision arithmetic on the National Central University VAX 8650 and HP 730 computers. The order of the Prandtl numbers associated with electronic materials grown by the float-zone method is less than 10^{-1}, such as *Si* ($Pr = 0.02$) and *Ga As* ($Pr = 0.068$). Therefore, calculations were performed for $Pr < 1$ with a wide range of aspect ratios.

In *Figure 4*, the critical Marangoni number Ma_c is plotted as a function of aspect ratio A for $Pr = 0.1$, $Bi = 0.3$, $Gr = 0$, and case (1). The results are compared with the energy-theory results

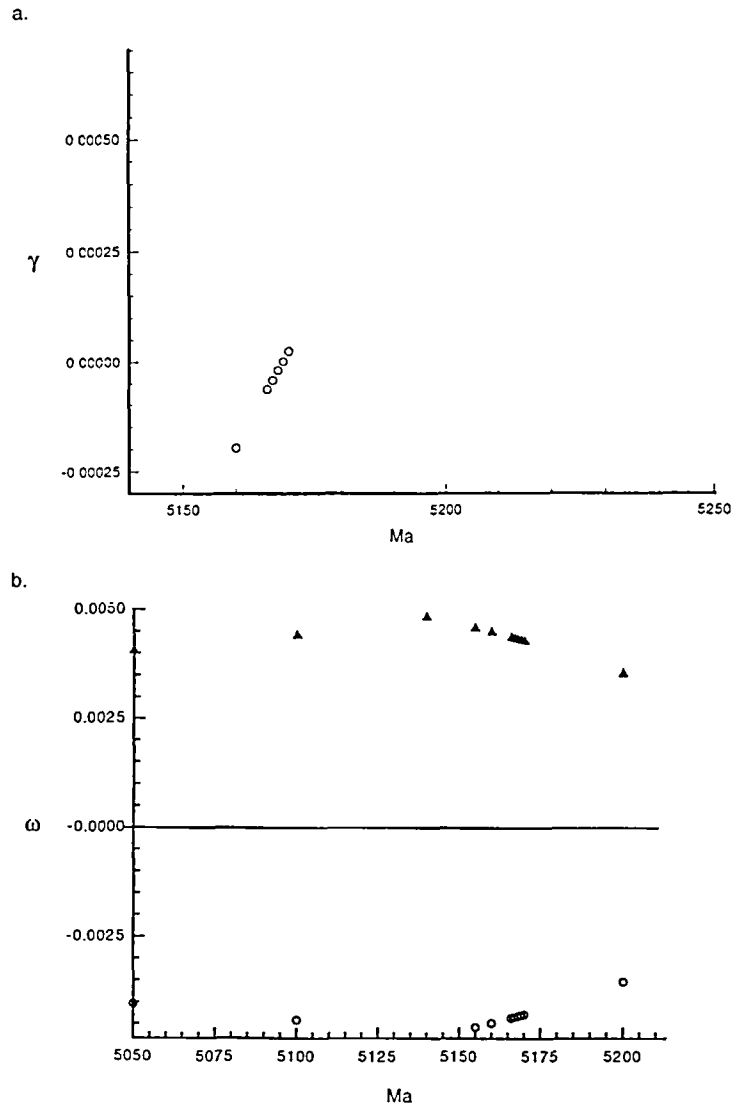

Figure 1 Variation of Ma with σ for case (I), $Pr = 0.1$, $Bi = 0$, $Gr = 0$, and $A = 1$

of Shen *et al.*[14]. The critical Marangoni number Ma_c is strongly dependent on the aspect ratio A and increases as A increases. This is due to the stabilizing effect generated by the existence of the endwalls. Due to the shape instability of the liquid bridge, the bridge will break down before its length reaches the Rayleigh limit $(2\pi R)$[7]. From *Figure 4*, it is clear that the present results are in qualitative agreement with the energy-theory results. As expected, the critical Marangoni number calculated by the linear theory is higher than that predicted by the energy theory, since the linear-theory results provide sufficient conditions for instability, while the energy-theory results give sufficient conditions for stability.

Recently, Velten *et al.*[11] conjectured that the thermocapillary convection in cylindrical liquid bridges may be destabilized by reducing the radial heat loss along the free surface. To verify

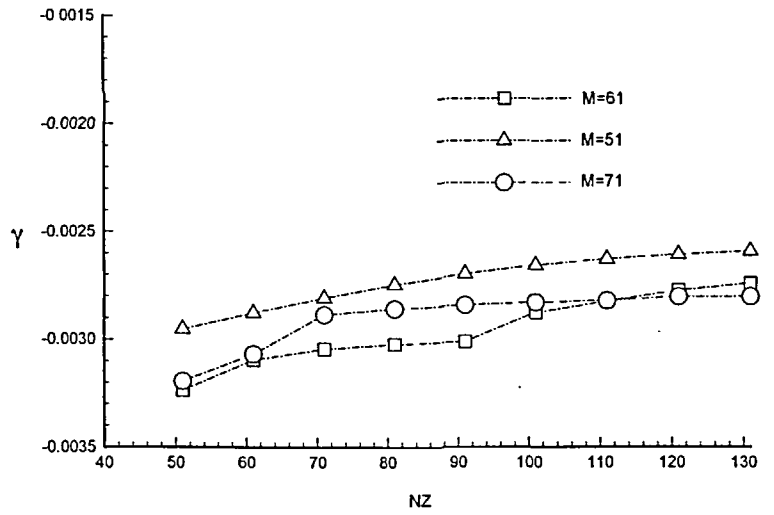

Figure 2 Growth rate γ versus number of finite-difference grid points for $Pr = 0.1$, $Bi = 0.3$, $A = 1$, $Gr = 0$, $Ma = 2000$, $N = 9$, and case (I)

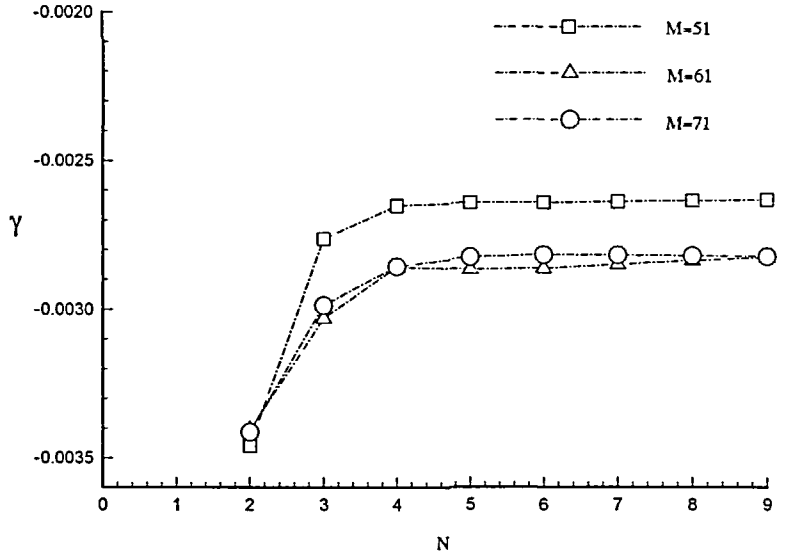

Figure 3 Growth rate γ versus number of trial-function terms N for $Pr = 0.1$, $Bi = 0.3$, $A = 1$, $Gr = 0$, $Ma = 2000$, $Nz = 111$, and case (I) with three different numbers for finite-difference grid points M

this opinion, we have investigated the influence of the Biot number and the form of the ambient temperature distribution on the critical Marangoni number. *Figure 5* shows the critical Marangoni number Ma_c versus A for $Pr = 0.1$, $Gr = 0$ and case (I) with four different Biot numbers. Because the disturbances decay faster due to better heat transfer along the free surface, the critical Marangoni number increases with increasing Bi. The influence of the Biot number on the critical Marangoni number is enhanced by the decreasing aspect ratio. This is due to the higher heat transfer rate for lower aspect ratio since the heat transfer area for lower aspect ratios is larger

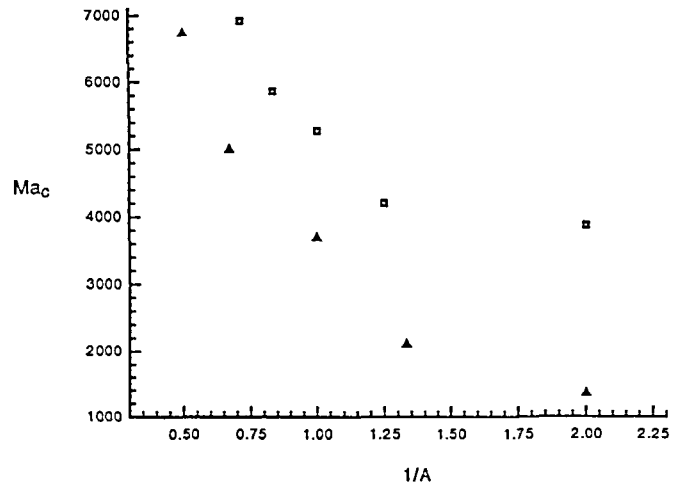

Figure 4 Critical Marangoni number Ma_c versus aspect ratio A for $Pr = 0.1$, $Bi = 0.3$, $Gr = 0$, and case (I). The triangle represents the results of energy method[14] and the square represents the present results

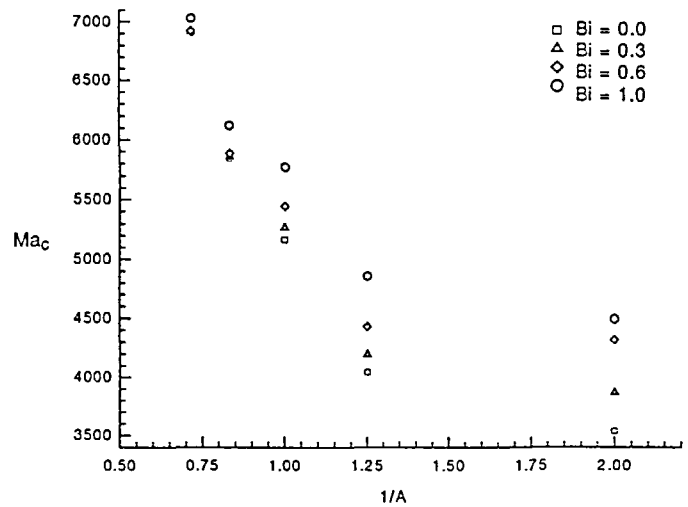

Figure 5 Critical Marangoni number Ma_c versus aspect ratio A for $Pr = 0.1$, $Gr = 0$, and case (I) with different Bi

Table 1 Grid distribution for different aspect ratios using in the basic-state computations

A	M	NZ
0.5	51	101
0.7	51	101
0.8	51	101
1.0	61	101
1.2	61	91
1.4	71	91
1.5	71	91

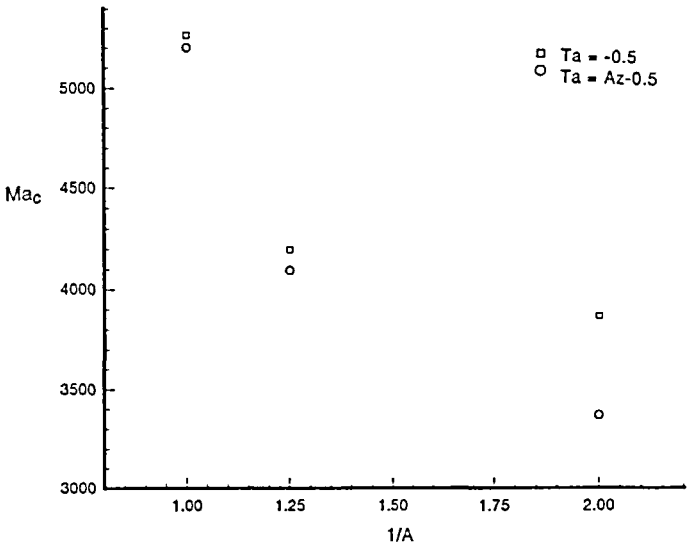

Figure 6 Critical Marangoni number Ma_c versus aspect ratio A for $Pr = 0.1$, $Gr = 0$, and $Bi = 0.3$ with two different ambient temperature distributions

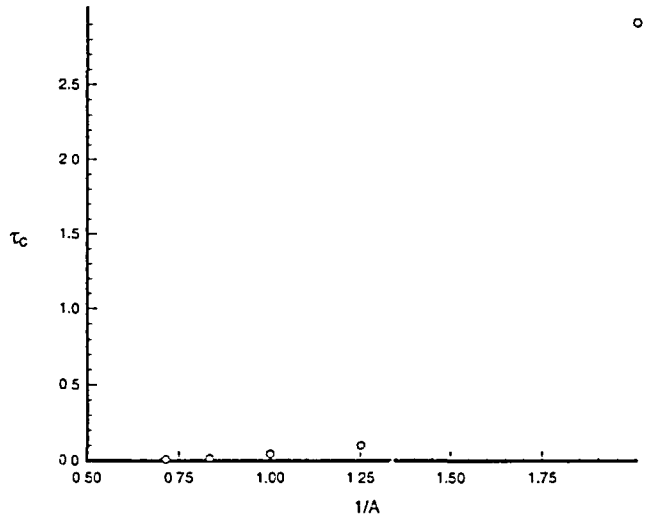

Figure 7 Oscillation period at the marginal state versus aspect ratio A for $Pr = 0.1$, $Bi = 0.3$, $Gr = 0$, and case (I)

than for higher aspect ratios. *Figure 6* illustrates that the critical Marangoni number is affected by the form of the ambient temperature distribution. The critical Marangoni numbers for case (I) are higher than those of case (II). This is expected because the heat transfer along the free surface for case (I) is better than that for case (II) when all the parameters are fixed.

The oscillation period at the marginal state is defined as $\tau_c = 1/(Ma\,A^2)$. The influence of the aspect ratio on the period of oscillation is shown in *Figure 7*. From *Figure 7*, it is clear that the oscillatory period increases as the aspect ratio decreases. The magnitude of the oscillatory period is dependent on the flow speed on the free surface and the aspect ratio. The time required for

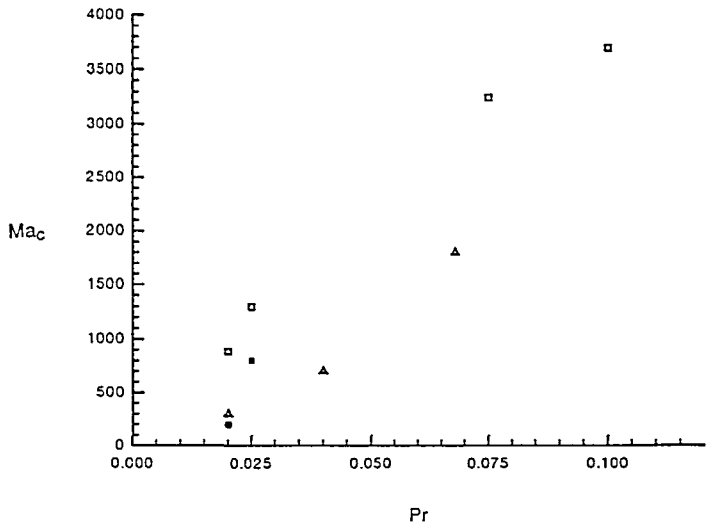

Figure 8 Critical Marangoni number Ma_c versus Prandtl number Pr for $Bi = 0$, $Gr = 0$, $A = 0.8$, and case (I). The squares represent the present results and the triangles represent the numerical results of Rupp, Müller and Neumann[13]. The solid circles and the solid triangle denote the experimental results of Jurisch and Löser[2] and Cröll and Müller-Sebert[13], respectively

one revolution in a thermocapillary convection cell decreases as the surface speed and aspect ratio increase. Hence, both effects reduce the magnitude of the oscillation period. The flow speed on the free surface increases as the Marangoni number increases. Therefore, the results in *Figure 7* can be expected, since the critical Marangoni number increases with increasing A. The experimental results of Velten *et al.*[11] also show similar trends.

The effect of the Prandtl number on the critical Marangoni number Ma_c is of interest. *Figure 8* is a plot of Ma_c versus Pr for $Bi = 0$, $Gr = 0$, $A = 0.8$, and case (I). The triangles represent the numerical results predicted by Rupp, Müller and Neumann[13], while the solid circle and the solid square refer to the experimental results obtained by growing Mo crystals[2] and Si crystals[13], respectively. The present results are consistent with those of numerical calculations[13] and experimental observations[2,13] in that the critical Marangoni number increases as the Prandtl number increases. The critical Marangoni numbers predicted by the present method are higher than those from experiment observations and obtained in numerical simulations.

CONCLUSIONS

Linear-stability analysis has been used to study the instability of thermocapillary convection in a nonisothermal liquid bridge for axisymmetric disturbances. A mixed finite difference-spectral method has been developed to solve the linear disturbance equations. The present results are in qualitative agreement with those of energy-stability analysis, those of numerical computations, and of experimental observations. Based on the present results, enhancing radial heat transfer at the free surface, which can be reached by increasing Bi or changing the ambient temperature distribution, increases stability. This result confirms the conjecture of Velten *et al.*[11] To obtain results that are in better agreement with the experiment observations, the present method shall be able to take into account the effect of nonaxisymmetric disturbances and further investigates the influence of thermal conditions in the surrounding environment, e.g. thermal radiation and ambient temperature distribution. When the non-axisymmetric disturbances are considered, the

disturbance equations become three-dimensional. The mixed finite difference-spectral procedure will yield a complex eigenvalue system which is much bigger than the present two-dimensional case. Therefore, the large computer memory and computation time are required by the three-dimensional case. The development of the three-dimensional one is currently under way.

ACKNOWLEDGEMENT

This research is supported by the National Science Council of the R.O.C. under Grant No. NSC79-0401-E008-17.

REFERENCES

1 Schwabe, D., Scharmann, A., Preisser, F. and Oeder, R. Experiments on surface tension driven flow in floating zone melting, *J. Crystal Growth*, **43**, 305–312 (1978)
2 Jurisch, M. and Löser, W. Analysis of periodic non-rotational W striations in Mo single crystals due to nonsteady thermocapillary convection, *J. Crystal Growth*, **102**, 214–222 (1990)
3 Xu, J.-J. and Davis, S. H. Liquid bridges with thermocapillarity, *Phys. Fluids*, **26**, 2880–2886 (1983)
4 Kuhlmann, H. Small amplitude thermocapillary flow and surface deformations in a liquid bridge, *Phys. Fluids A*, **1**, 672–677 (1989)
5 Chang, C. E. and Wilcox, W. R. Analysis of surface tension driven flow in floating zone melting, *Int. J. Heat Mass Transfer*, **19**, 335–366 (1976)
6 Fu, B. and Ostrach, S. Numerical solution of thermocapillary flows in floating zones, in *Transport Phenomena in Materials Processing, Power Eng. Div.*, **10**, *Heat Transfer Div.*, **29**, 1 ASME (1985)
7 Chen, J.-C., Sheu, J.-C. and Lee, Y.-T. Maximum stable length of nonisothermal liquid bridges, *Phys. Fluids A*, **2**, 1118–1123 (1990)
8 Chun, C.-H. Experiments on steady and oscillatory temperature distribution in a floating zone due to the Marangoni convection, *Acta Astronautic*, **7**, 479–488 (1980)
9 Preisser, F., Schwabe, D. and Scharmann, A. Steady and oscillatory thermocapillary convection in liquid columns with free cylindrical surface, *J. Fluid Mech.*, **126**, 545–567 (1983)
10 Kamotani, Y., Ostrach, S. and Vargas, M. Oscillatory thermocapillary convection in a simulated floating-zone configuration, *J. Crystal Growth*, **66**, 83–90 (1984)
11 Velten, R., Schwabe, D. and Scharmann, A. The periodic instability of thermocapillary convection in cylindrical liquid bridges, *Phys. Fluids A*, **3**, 267–279 (1991)
12 Xu, J.-J. and Davis, S. H. Convective thermocapillary instabilities in liquid bridges, *Phys. Fluids*, **27**, 1102–1107 (1984)
13 Rupp, R., Müller, G. and Neumann, G. Three dimensional time dependent modelling of Marangoni convection in zone melting configurations for GaAs, *J. Crystal Growth*, **97**, 34–41 (1989)
14 Shen, Y., Neitzel, G. P., Jankowski, D. F. and Mittelman, H. D. Energy stability of thermocapillary convection in a model of the float-zone, crystal-growth process, *J. Fluid Mech.*, **217**, 639–660 (1990)
15 Neitzel, G. P., Law, C. C., Jankowski, D. F. and Mittelman, H. D. Energy stability of thermocapillary convection in a model of the float-zone crystal-growth process. II: Nonaxisymmetric disturbances, *Phys. Fluids A*, **3**, 2841–2846 (1991)
16 Neitzel, G. P., Chang, K.-T., Jankowski, D. F. and Mittelman, H. D. Linear stability of thermocapillary convection in a model of the float-zone crystal growth, *AIAA paper no. 92-0604* (1992)
17 McDonough, J. M. and Catton, I. A mixed finite difference-Galerkin procedure for two-dimensional convection in a square box, *Int. J. Heat Mass Transfer*, **75**, 54–72 (1988)
18 Chen, J.-C., Sheu, J.-C. and Jwu, S.-S. Numerical computation of thermocapillary convection in rectangular cavity, *Numer. Heat Transfer A*, **17**, 287–308 (1990)
19 Chen, J.-C. and Chen, J.-Y. Linear Marangoni instability of a fluid in circular cylindrical containers, *IAF paper no. 91-393* (1991)
20 Harris, D. L. and Reid, W. H. On orthogonal functions which satisfy four boundary conditions – II. Integrals for use with Fourier-type expansion, *Astrophys. J. Supp. Ser.*, **3**, 448–452 (1958)

APPENDIX A

$$[\mathbf{M}_{11}]_{jk} = -\int_{z=0}^{1/A} \frac{A_j}{r} \cdot A_k \, dz$$

$$[\mathbf{M}_{12}]_{jk} = \int_{z=0}^{1/A} \left(\frac{z}{r^2} + \frac{Re\, U}{r}\right) A_j \cdot A_k \, dz$$

$$[\mathbf{M}_{13}]_{jk} = \int_{z=0}^{1/A} \left\{\left[-\frac{3}{r^3} - \frac{2}{r^2} Re\, U + \frac{Re}{r}(U_r + W_z)\right] + \frac{Re\, W}{r} D_z - \frac{2}{r} D_z^2\right\} A_j \cdot A_k \, dz$$

$$[\mathbf{M}_{14}]_{jk} = \int_{z=0}^{1/a} \left\{\left[\frac{3}{r^4} + \frac{2Re\, U}{r^3} - \frac{Re}{r^2}(U_r - W_z) - \frac{Re}{r}(U_{zz} - W_{rz})\right] - \frac{Re\, W}{r^2} D_z + \left(\frac{2}{r} + \frac{Re\, U}{r}\right) D^{2z?}\right\} A_j \cdot A_k \, dz$$

$$[\mathbf{M}_{15}]_{jk} = \int_{z=0}^{1/a} Re\left[-\frac{1}{r^2}(U_z - W_r) + \left(\frac{1}{r} U_{rz} - \frac{1}{r} W_{rr}\right)\right] D_z A_j \cdot A_k \, dz + \int_{z=0}^{1/a} Re\left[\frac{1}{r}(W_z - U_r) - \frac{U}{r^2}\right] D_z^2 A_j \cdot A_k \, dz + \int_{z=0}^{1/a} \frac{Re\, W}{r} D_z^3 A_j A_k \, dz - \int_{z=0}^{1/a} \frac{1}{r} D_z^4 A_j \cdot A_k \, dz$$

$$[\mathbf{M}_{16}]_{jk} = \frac{Gr}{Re} \int_{z=0}^{1/a} B_j \cdot A_k \, dz$$

$$[\mathbf{N}_{11}]_{jk} = Re \int_{z=0}^{1/a} \frac{A_j}{r} \cdot A_k \, dz$$

$$[\mathbf{N}_{12}]_{jk} = Re \int_{z=0}^{1/a} -\frac{1}{r^2} A_j \cdot A_k \, dz$$

$$[\mathbf{N}_{13}]_{jk} = Re \int_{z=0}^{1/a} \frac{D_z^2 A_j}{r} \cdot A_k \, dz$$

$$[\mathbf{M}_{21}]_{jk} = Ma \int_{z=0}^{1/a} B_j \cdot B_k \, dz$$

$$[\mathbf{M}_{22}]_{jk} = -\frac{Ma}{r} \int_{z=0}^{1/a} T_z A_j \cdot B_k \, dz$$

$$[\mathbf{M}_{23}]_{jk} = \frac{Ma}{r} T_r \int_{z=0}^{1/a} D_z A_j \cdot B_k \, dz$$

$$[\mathbf{M}_{24}]_{jk} = -\int_{z=0}^{1/a} B_j \cdot B_k \, dz$$

$$[\mathbf{M}_{25}]_{jk} = \int_{z=0}^{1/a} \left(Ma\, U - \frac{1}{r}\right) B_j \cdot B_k \, dz$$

$$[\mathbf{M}_{26}]_{jk} = -\int_{z=0}^{1/a} (Ma\, W D_z - D_z^2) B_j \cdot B_k \, dz$$

$$[\mathbf{M}_b]_{jk} = \int_{z=0}^{1/a} D_z B_j \cdot A_k \, dz$$

APPENDIX B

$$[\bar{M}_{11}]_{kj} = \frac{[M_{11}]_{kj}}{\Delta r^4} + \frac{[M_{12}]_{kj}}{2\Delta r^3}$$

$$[\bar{M}_{12}]_{kj} = -\frac{4[M_{11}]_{kj}}{\Delta r^4} - \frac{[M_{12}]_{kj}}{\Delta r^3} + \frac{[M_{13}]_{kj}}{\Delta r^2} + \frac{[M_{14}]_{kj}}{2\Delta r}$$

$$[\bar{M}_{13}]_{kj} = \frac{6[M_{11}]_{kj}}{\Delta r^4} - \frac{2[M_{13}]_{kj}}{\Delta r^2} + [M_{15}]_{kj}$$

$$[\bar{M}_{14}]_{kj} = -\frac{4[M_{11}]_{kj}}{\Delta r^4} + \frac{[M_{12}]_{kj}}{\Delta r^3} + \frac{[M_{13}]_{kj}}{\Delta r^2} - \frac{[M_{14}]_{kj}}{2\Delta r}$$

$$[\bar{M}_{15}]_{kj} = \frac{[M_{11}]_{kj}}{\Delta r^4} - \frac{[M_{12}]_{kj}}{2\Delta r^3}$$

$$[\bar{M}_{16}]_{kj} = \frac{[M_{16}]_{kj}}{2\Delta r}$$

$$[\bar{M}_{17}]_{kj} = -\frac{[M_{16}]_{kj}}{2\Delta r}$$

$$[\bar{M}_{21}]_{kj} = -[M_{21}]_{kj}$$

$$[\bar{M}_{22}]_{kj} = \frac{[M_{22}]_{kj}}{2\Delta r}$$

$$[\bar{M}_{23}]_{kj} = [M_{23}]_{kj}$$

$$[\bar{M}_{24}]_{kj} = \frac{-[M_{22}]_{kj}}{2\Delta r}$$

$$[\bar{M}_{25}]_{kj} = \frac{[M_{24}]_{kj}}{\Delta r^2} + \frac{[M_{25}]_{kj}}{2\Delta r}$$

$$[\bar{M}_{26}]_{kj} = -\frac{2[M_{24}]_{kj}}{\Delta r^2} + [M_{26}]_{kj}$$

$$[\bar{M}_{27}]_{kj} = \frac{[M_{24}]_{kj}}{\Delta r^2} - \frac{[M_{25}]_{kj}}{2\Delta r}$$

$$[\bar{N}_{11}]_{kj} = -\left(\frac{[N_{11}]_{kj}}{\Delta r^2} + \frac{[N_{12}]_{kj}}{2\Delta r}\right)$$

$$[\bar{N}_{12}]_{kj} = \left(\frac{2[N_{11}]_{kj}}{\Delta r^2} - [N_{13}]_{kj}\right)$$

$$[\bar{N}_{13}]_{kj} = -\left(\frac{[N_{11}]_{kj}}{\Delta r^2} - \frac{[N_{12}]_{kj}}{2\Delta r}\right)$$